JOURNAL OF COMPUTATIONAL PHYSICS **147,** 545–567 (1998)
ARTICLE NO. CP986101

On Godunov-Type Schemes for Magnetohydrodynamics

1. A Model System

R. S. Myong* and P. L. Roe†, ‡

*NASA Goddard Space Flight Center, Mail Stop 930, Greenbelt, Maryland 20771; †W. M. Keck Foundation Laboratory for CFD, Department of Aerospace Engineering, University of Michigan, Ann Arbor, Michigan 48109
E-mail: myong@lucullus.gsfc.nasa.gov, philroe@engin.umich.edu

Received February 10, 1998; revised September 15, 1998

In the light of recent analytical results on the MHD Riemann problem, Godunov-type numerical schemes for magnetohydrodynamics (MHD) are revisited. As the first step, a model system that exactly preserves the MHD hyperbolic singularities is considered. For this model, analytical results on shock waves are summarized and critical problems occurring in developing shock-capturing methods are identified. Using the results, we propose a new way to define fluxes on cell interfaces. It consists of two solvers, one on the well-posed Riemann problem and another on the evolution of Alfvén waves. Numerical experiments show that the new scheme is more efficient in calculating large-time solutions.

Key Words: Godunov-type schemes; conservation laws, magnetohydrodynamics.

1. INTRODUCTION

As numerical simulations come to play a vital role in studying the motion of ionized gases in hypersonic flows [4, 33], space propulsion [42], and space physics [15], great emphasis has been placed on the development of numerical schemes for the system of magnetohydrodynamic equations. Out of the various possibilities, Godunov-type schemes—encouraged by successful applications to the Euler equations—are considered to be highly effective in resolving discontinuities such as shock waves for high speed flow problems. These schemes were pioneered by Godunov [22] who used the local characteristic structure obtained from

‡Present address: Centre pour Mathematiques et leurs Applications/CNRS, Ecole normale Superieure de Cachan, 61 avenue du Président Wilson, 94235 Cachan Cedex, France.

0021-9991/98 $25.00

solving the Riemann problem to define a upwind method. The basic building blocks can be easily adapted to problems in higher space dimensions through the finite-volume approach.

Initially, application to the MHD equations seems to be straightforward. Brio and Wu [8] developed an approximate MHD Riemann solver based on Roe's scheme. Zachary and Colella [45] developed a higher-order Godunov method for ideal magnetohydrodynamics. Dai and Woodward [13, 14] presented an approximate Riemann solver which treats all waves emanating from the initial discontinuity as themselves discontinuous. van Putten [41] applied Roe's scheme to fully relativistic planar MHD shock problems. Cargo and Gallice [9, 10] constructed a Roe's matrix which is valid for arbitrary ratio of specific heats. Aslan [3] carried out one-dimensional simulation of MHD waves using Roe's solver.

However, it soon becomes apparent that the wave structure in MHD is far more complicated than that in gas dynamics, in that there exist hyperbolic singularities where the MHD eigensystem is not well behaved. There have been two schools of thought on the numerical effects of these singularities. One is that the effect on the Riemann solution is not global, so that all the problems can be handled merely by a conservative discretization. All of the above works fall under this category. The other is that the effect is global, so that Godunov-type schemes that do not explicitly account for the special character of MHD waves are inappropriate. The difficulty was demonstrated for a simple nonstrictly hyperbolic system by Tveito and Winther [39]. They argued that a piecewise constant approximation generates a solution with erroneous qualitative behavior. Similarly, it was implied by Freistühler [18, 19] that precise control of the numerical dissipation is crucial for generating the correct numerical solutions. However, none of these could provide definite recipes for treating MHD singularities, whose behavior, essentially the problem of shock admissibility, has not been well-understood.

The study of the admissibility of MHD shock waves has a long history [21, 12, 20, 44]. Since an explicit form of the MHD Rankine–Hugoniot relations was derived in the late 1950s [6], it has remained as a lingering source of debate. In particular, the question of whether the intermediate shocks, which are defined as shocks that change the orientation of the transverse fields, can exist in the real world has been a hotly debated issue. In the past, all the intermediate shocks were considered nonphysical by the so-called evolutionary theory [1, 2, 27, 34], an MHD version of the Lax condition [28]. This theory restricts physically relevant shocks to those across which only one family of characteristics converges.

Contrary to this theory, it was shown in a recent series of numerical computations by Wu [43, 44] that some intermediate shocks can exist, although the rotational discontinuity (a discontinuous wave that changes only the direction) cannot exist. A similar conclusion was drawn in an analytical study of Freistühler [17]. Even an observation of an intermediate interplanetary shock has been reported by Chao *et al.* [11].

However, criticisms of physical relevance of intermediate shocks still persist. For example, Markovskii and Somov [29] argued that intermediate shocks are only realizable if their disintegration into a set of evolutionary discontinuities is forbidden for some reason. From the numerical viewpoint, Barmin *et al.* [5] and Dai and Woodward [13] argued that numerical viscosity can produce intermediate shocks and thus they must not be considered physically relevant. In these arguments, the theoretical justification for banishing intermediate shocks is the evolutionary theory; intermediate shocks are unstable against rotational perturbation.

In an attempt to solve this controversy, we started an analytical study of intermediate shocks [30–32]. The study was based on a 3×3 model set of conservation laws that share

the singularity structure of the MHD equations, and it is that model that we study numerically in the present paper. However, all important conclusions go over to the MHD equations. In that study, we showed that all entropy-satisfying intermediate shocks have viscous profiles, which suggests that they may sometimes be allowable. We also found that the nonplanar MHD Riemann problem is not well-posed, whereas the planar MHD Riemann problem (where both solution vectors, the velocity and the magnetic field, are assumed to lie in one plane) is actually well-posed despite using intermediate shocks to allow the transverse field to change sign. We also gave formulae that allow the exact solution to be constructed, although very lengthy iteration is involved. In the nonplanar problem multiple solutions can exist for given data. Choosing the correct solution could involve knowing the details of the physical dissipation and also having some information about the structure of the data beyond regarding it as just a discontinuity.

Our conclusions can be expressed as follows. Nonevolutionary shocks—some of them compound waves—in general disintegrate at sufficiently large times into regular shocks and Alfvén waves, unless they cause rotation by a multiple of π. In that case, they may persist if they have the correct internal structure. For a particular form of dissipation we were able to indicate this structure. Thus weak solutions involving intermediate shocks should in these special cases be allowed in numerical solutions of both the planar and nonplanar Riemann problem. In the planar problem they are automatically stabilized by the absence of any out-of-plane components in the computation. This was the case with the compound wave discovered by Brio and Wu [8].

In nonplanar problems, intermediate shocks may appear unpredictably in numerical solutions, since numerical schemes have their own kind of dissipation that may not select the same set of weak solutions selected by the physical dissipation. In cases of uncertainty there seems to be no alternative to using a grid fine enough to resolve the internal structure and including the dissipative effects in the discretization.

However, there is one likely scenario in which a short cut is still possible. If we assume that the physical dissipation is such as almost always to cause the eventual disintegration of all nonevolutionary waves, and if we assume that our interest is in obtaining the solution at large times, then the numerical scheme should encourage nonevolutionary waves to break up as quickly and cleanly as possible. This point is exactly how the strategy for developing MHD codes in this paper differs from the previous works. Nevertheless, if nonevolutionary waves are enforced, for example by symmetry, then our scheme is capable of computing them.

Our strategy can be summarized as follows. From general left and right states, we identify a modified Riemann problem that is well-posed and for which an approximate Riemann solver can be easily constructed. From this, we calculate intermediate states and into these insert the Alfvén waves. Finally, from this information we calculate fluxes on cell surfaces. This scheme can allow intermediate shocks as weak solutions, but it will not violate any physical laws. Numerical solutions can converge to large-time solutions more quickly than with previous methods since the transverse field is described more accurately.

This paper will pursue these topics for a model system that exactly preserves the singularities of the MHD system. It is organized as follows. In Section 2, we summarize the analytical results on the Riemann problem. In particular, we present a viscosity admissibility condition that allows the existence of intermediate shocks. For numerical verification, several exact solutions of Riemann problem are given. In Section 3, we propose a new scheme based on the well-posed Riemann problem, and numerical implementation of an entropy condition is discussed. In Section 4, several numerical results are presented in

order to demonstrate the property of the new scheme. Finally, in Section 5, we discuss the possibility of extending the new scheme to the actual MHD system and discuss what the effects of that extension might be.

2. THEORY OF THE RIEMANN PROBLEM FOR THE MHD MODEL

A close look at MHD waves suggests that they may be described concisely in a three-dimensional phase space consisting of p, B_y, B_z [7, 23, 31]. A 3×3 model system exactly preserving the MHD singularities was derived,[1]

$$\mathbf{u}_t + \mathbf{f}_x = \mathbf{d}\mathbf{u}_{xx}, \tag{2}$$

where

$$\mathbf{u} = \begin{pmatrix} u \\ v \\ w \end{pmatrix}, \quad \mathbf{f} = \begin{pmatrix} cu^2 + v^2 + w^2 \\ 2uv \\ 2uw \end{pmatrix}, \quad \mathbf{d} = \begin{pmatrix} \mu & 0 & 0 \\ 0 & \eta & -\chi \\ 0 & \chi & \eta \end{pmatrix}. \tag{3}$$

The longitudinal viscosity μ, the magnetic resistivity η are the dissipative coefficients, while the Hall coefficient χ is a dispersive coefficient. Since we can obtain a large body of analytic results for this system, it can serve as a test bed for developing various numerical schemes. We present here only an outline of the more complete analysis available in [26, 31].

2.1. *Eigensystem*

The model system yields three waves, which can be described as Alfvén, fast and slow; their speeds are given by

$$\lambda_a = 2u, \quad \lambda_{f,s} = (c+1)u \pm \left((c-1)^2u^2 + 4(v^2+w^2)\right)^{1/2}, \tag{4}$$

always satisfying $\lambda_s \le \lambda_a \le \lambda_f$. One of $\lambda_{s,f}$ vanishes when $v^2 + w^2 = cu^2$. These waves can be thought of as the set of MHD waves that run wholly to the right of the contact discontinuity, but note that the wavespeeds as defined here may be negative. The normalized left and right eigenvectors are

$$\mathbf{l}_{s,a,f} = \begin{pmatrix} -\alpha_f S & \alpha_s v' & \alpha_s w' \\ 0 & w' & -v' \\ \alpha_s S & \alpha_f v' & \alpha_f w' \end{pmatrix}, \quad \mathbf{r}_{s,a,f} = \begin{pmatrix} -\alpha_f S & 0 & \alpha_s S \\ \alpha_s v' & w' & \alpha_f v' \\ \alpha_s w' & -v' & \alpha_f w' \end{pmatrix}. \tag{5}$$

Here several nondimensional quantities are introduced;

$$\alpha_f^2 = \frac{\lambda_a - \lambda_s}{\lambda_f - \lambda_s}, \quad \alpha_s^2 = \frac{\lambda_f - \lambda_a}{\lambda_f - \lambda_s}, \quad v' = \frac{v}{r}, \quad w' = \frac{w}{r}, \quad S = \mathrm{sign}(\alpha_f \alpha_s), \tag{6}$$

[1] Here the correspondences to the MHD system are satisfied,

$$c = \gamma + 1, \quad u = \left(\frac{a}{c_a}\right)^2 - 1, \quad v = \frac{B_y}{B_x}, \quad w = \frac{B_z}{B_x},$$

where $c_a = \tau^{1/2}|B_x|$ is the Alfvén wave speed, $a = \sqrt{\gamma \tau p}$ is the acoustic wave speed, p is the pressure, and τ is the specific volume. $B_{x,y,z}$ are x, y, z components of the magnetic field. The proof of $c = \gamma + 1$ can be found in Appendix C of [32]. For physically relevant cases $\gamma \ge 1$, where γ is the ratio of specific heats, and so $c \ge 2$. For algebraic simplicity we will often take $c = 3$.

where $re^{i\phi} = v + iw$. Compare with $\alpha_{f,s}$, $\beta_{y,z}$ in the MHD equations [38],

$$\alpha_f^2 = \frac{1 - q_s}{q_f - q_s}, \quad \alpha_s^2 = \frac{q_f - 1}{q_f - q_s}, \quad \beta_{y,z} = \frac{B_{y,z}}{B_\perp}, \tag{7}$$

where $q_{f,s} = c_{f,s}^2/a^2$ and $B_\perp^2 = B_y^2 + B_z^2$. $c_{f,s}$ represent fast and slow magnetoacoustic wave speeds. For $\alpha_{f,s}$, there exists symmetry in the relationships

$$\alpha_s^2 + \alpha_f^2 = 1, \quad \alpha_s \alpha_f = \frac{2r}{\lambda_f - \lambda_s} S. \tag{8}$$

As with the MHD eigensystem, there are some cases that can potentially cause trouble. First, quantities v', w' are indeterminate if $r = 0$. In a theory that treats only small disturbances they may be given arbitrary values, provided their squares sum to unity $v' = \cos\phi$, $w' = \sin\phi$, but this is unconvincing if a small value of r arises numerically as an average of two large neighboring values. It will be seen later that our treatment largely removes this singularity.

Second, $\alpha_{f,s}$ become indeterminate near the *umbilic* point $u = r = 0$ at which $\lambda_s = \lambda_a = \lambda_f$; that is, all three waves resonate. However, since $\alpha_s^2 + \alpha_f^2 = 1$, the eigenvectors cannot be singular. Near the singularity, $\alpha_{f,s}$ can be shown to equal

$$\alpha_f^2 = \sin^2\frac{\theta}{2}, \quad \alpha_s^2 = \cos^2\frac{\theta}{2}, \tag{9}$$

where $\theta = \tan^{-1}(2/(c-2)(r/u))$, but although this clarifies the nature of the singularity it does not remove it. The singularity is somewhat benign; Roe and Balsara [38] showed that any error in evaluating $\alpha_{f,s}$ near the umbilic point was not magnified in any corresponding error in the numerical flux. In the present treatment, Riemann problems close to the umbilic point are avoided unless both states are close to the umbilic point.

2.2. *Rankine Hugoniot and Shock Admissibility Conditions*

The admissibility of MHD shock waves has been a matter of much debate over the years [1, 27]. Recently, we developed a global theory for the model and MHD systems [31, 32] that distinguishes between planar and nonplanar problems. However, in both cases it is required that admissible shocks have viscous profiles. Here the planar problem means that there exists no w component; in other words, everything is confined in flatland. As a result, there exists no Alfvén wave in the planar problem. On the other hand, nonplanar problems are of two types: coplanar problem with end states in the same plane and nonzero w components and noncoplanar problem.

2.2.1. Planar shocks. Travelling shock-wave solutions satisfy the Hugoniot condition $[\mathbf{f}] = s[\mathbf{u}]$, where s represents the shock speed. For the planar model problem, the Rankine–Hugoniot relation is obtained by eliminating s; it is

$$\overline{v}[u]^2 + (1-c)\overline{u}[u][v] - \overline{v}[v]^2 = 0, \tag{10}$$

where the overbars indicate arithmetic averages taken across the discontinuity and $[Q]$ denotes the jump of a quantity Q, that is, $(Q_R - Q_L)$. Throughout this paper we reserve

L, R for downstream and upstream states. For left and right states, we will use subscripts l, r. By this definition, $L = l$ and $R = r$ for right-running waves, but $L = r$ and $R = l$ for left-running waves. Since only waves propagating to the right with respect to the fluid are represented in the present model, $L = l$ and $R = r$. Shock speeds can be found from the eigenvalue equation

$$\lambda_{f,s} = (c+1)\bar{u} \pm \left((c-1)^2\bar{u}^2 + 4\bar{v}^2\right)^{1/2}. \tag{11}$$

Since for quadratic conservation laws, the so-called midpoint rule holds [26];

$$s_{f,s}(\mathbf{u}_L, \mathbf{u}_R) = \lambda_{f,s}(\bar{\mathbf{u}}), \tag{12}$$

where $\bar{\mathbf{u}} = \frac{1}{2}(\mathbf{u}_L + \mathbf{u}_R)$. The four parameters $(\lambda_{f,s})_{L,R} - s$ determine the type of shocks. Only slow, fast, and overcompressive shocks were shown to be physically relevant by the viscosity admissibility condition in [31, 32], so that only these shocks should be found in numerical solutions. However, the undercompressive shocks do not have viscous profiles and so they must not appear in planar solutions.

2.2.2. Entropy production. Both the planar and nonplanar models possess an entropy $\sigma = u^2 + v^2 (+w^2)$ which satisfies

$$\sigma_t + g_x = 0, \tag{13}$$

where $g = 2u(cu^2/3 + v^2 + w^2)$ is the entropy flux. The increase of entropy across a discontinuity is easily found to be

$$-\frac{1}{6}[u]\left(c[u]^2 + 3[v]^2 + 3[w]^2\right),$$

so that the condition for entropy to increase is simply that $[u] < 0$. Throughout this paper, the phrase "entropy-satisfying" will be used to denote that this condition is met. However, the planar Riemann problem is well-posed only when we admit those shocks that are entropy-satisfying and also have viscous profiles, which excludes undercompressive shocks.

2.2.3. Nonplanar shocks. For the nonplanar model, the Hugoniot condition (10) is modified to read

$$\bar{r}[u]^2 + (1-c)\bar{u}[u][r] - \bar{r}[r]^2 = 0, \tag{14}$$

where $r^2 = v^2 + w^2$, and we also find that

$$[u](\bar{v}[w] - \bar{w}[v]) = 0, \tag{15}$$

which admits noncoplanar jumps only if $[u] = 0$; these are the Alfvén waves for which (from (14)) $[r] = 0$. In fact, the wave trajectories are all either coplanar ($v_L w_R = v_R w_L$) or purely rotational ($[u] = [v^2 + w^2] = 0$).

The signs of the six parameters $(\lambda_{f,a,s})_{L,R} - s$ determine which of the MHD characteristics run into the shock. In MHD terminology[2] the signs can be represented by four domains

[2] Shocks in MHD are characterized by an ordered pair of labels $(P \to Q)$, such that in the upstream state the shock speed s lies in region P and in the downstream state s lies in Q.

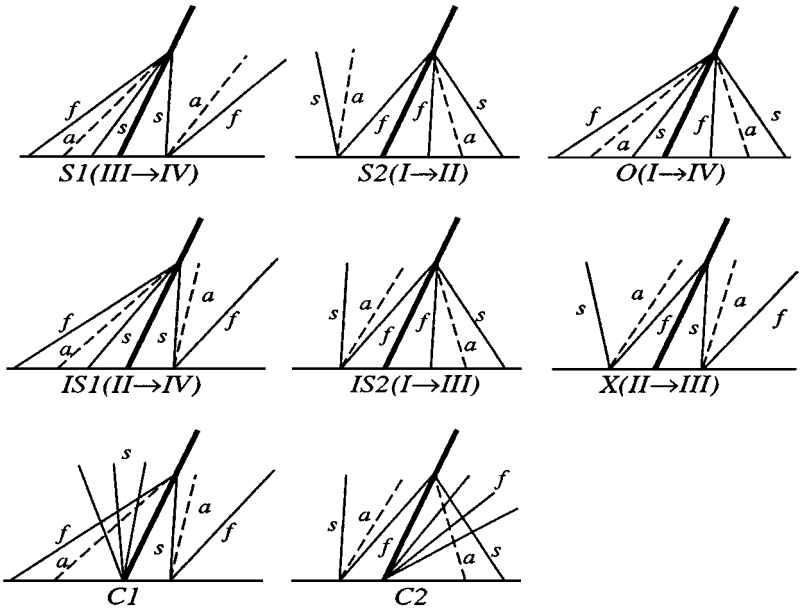

FIG. 1. Entropy-satisfying MHD waves having viscous profiles: S_1, S_2, regular shocks; IS_1, IS_2, O, X, intermediate shocks; C_1, C_2, slow, fast compound waves.

I–IV defined as

$$\text{IV} \quad \lambda_s \quad \text{III} \quad \lambda_a \quad \text{II} \quad \lambda_f \quad \text{I}.$$

In [31] it turned out that entropy satisfying regular shocks $S_1(\text{III} \to \text{IV})$, $S_2(\text{I} \to \text{II})$ and intermediate shocks $IS_1(\text{II} \to \text{IV})$, $IS_2(\text{I} \to \text{II})$, $O(\text{I} \to \text{IV})$, $X(\text{II} \to \text{III})$ all have viscous profiles. The principal difference between the planar and nonplanar analysis is that $X(II \to III)$ shocks have viscous profiles only in the nonplanar case. Entropy-satisfying MHD shocks having viscous profiles—some of which are embedded in compound waves—are illustrated in Fig. 1. Only $S_1(\text{III} \to \text{IV})$ and $S_2(\text{I} \to \text{II})$ shocks are considered physical in classical theory. In summary, contrary to the planar problem, the entropy condition $[u] < 0$ is equivalent for the nonplanar problem to the viscosity admissibility condition.

2.3. *Riemann Problem*

The Riemann problem concerns the evolution of an arbitrary initial discontinuity. The evolution can be described by various self-similar waves, contact discontinuity, and rarefaction waves, as well as shock waves. The model problem has no contact discontinuities. Planar rarefaction waves are described (when $c = 3$) by

$$J_{s,f} = u \pm (u^2 + v^2)^{1/2}, \tag{16}$$

$$\lambda_{f,s} = 4u \pm 2(u^2 + v^2)^{1/2} \tag{17}$$

$$= \frac{dx}{dt} = \frac{x}{t}, \tag{18}$$

where $J_{s,f}$ are the Riemann invariants such that $-\infty < J_f < 0$ for a fast wave and $0 < J_s < \infty$ for a slow wave. In passing through a rarefaction wave, the state vector (u, r)

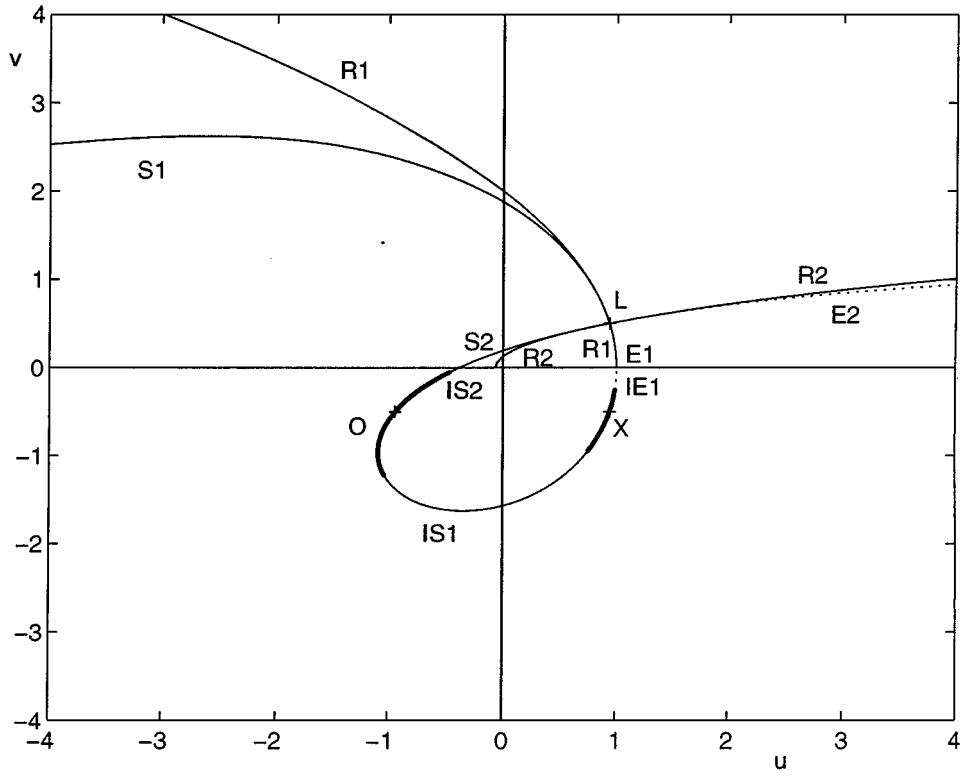

FIG. 2. Hugoniot locus and rarefaction-wave curves for a particular choice of the left state L. IE_1 represents IV $\rightarrow$ II expansive shock. The part of undercompressive shock (X) with $[u] < 0$ represents entropy-satisfying II $\rightarrow$ III shock, while the part with $[u] > 0$ represents entropy-violating III $\rightarrow$ II shock. The geometry of this diagram changes as L is placed in different regions of the plane; for more complete diagrams see [31].

traverses a parabola (see Fig. 2 and Eq. (16)), leading to the nonconvexity at $r = 0$, and the need to include compound waves to ensure a well-posed Riemann problem.

There are two types of compound waves: the slow compound wave, a slow rarefaction wave followed by an intermediate slow shock; and the fast compound wave, an intermediate fast shock followed by a fast rarefaction wave. The relationship between the shock and characteristics in compound waves is shown in Fig. 1. Using these compound waves, together with rarefactions, regular shocks, and overcompressive waves, it can be shown [26] that the planar Riemann problem is well-posed. Therefore, all shocks having viscous profiles, including ones embedded in compound waves, can appear in numerical solutions.

On the other hand, the Riemann problem becomes ill-posed in the nonplanar problem. This can be seen by noticing that for some data many solutions are possible, as will be shown in Section 2.4. They involve different internal structures that can be specified by, for example, the transverse field moment,

$$I_z \equiv \int_{-\infty}^{\infty} w \, dx. \tag{19}$$

This integral exists for coplanar data if one aligns the y-axis with the direction of the end-states. Otherwise, it can be defined by taking the limits of integration to be large but

finite, such that they lie in essentially uniform regions. In either case the third equation of the nonplanar model system yields

$$\frac{dI_z}{dt} + 2[uw] = 0. \tag{20}$$

When the end-states are coplanar and if the y-axis is aligned with the direction of the end-states ($w_L = w_R = 0$), I_z is invariant; but once the problem becomes noncoplanar, I_z becomes time-dependent.

2.4. *A Family of Riemann Problems with Nonunique Solutions*

For a planar Riemann problem whose left and right states are equal and opposite, $\mathbf{u}_L = -\mathbf{u}_R = (-u_0, v_0), u_0, v_0 > 0$, the analytical solution is C_1C_2 [31], a slow compound wave followed by a fast compound wave, described by

$$u = \frac{1}{3}\left(J_s + \frac{1}{2}\frac{x}{t}\right), \quad v = \left(\frac{J_s}{3}\left(J_s - \frac{x}{t}\right)\right)^{1/2} \qquad \text{for } -2(3u_0 + J_s) \le \frac{x}{t} < 0, \tag{21}$$

$$u = \frac{1}{3}\left(J_f + \frac{1}{2}\frac{x}{t}\right), \quad v = -\left(\frac{J_f}{3}\left(J_f - \frac{x}{t}\right)\right)^{1/2} \qquad \text{for } 0 < \frac{x}{t} \le 2(3u_0 - J_f). \tag{22}$$

An overcompressive shock with the speed $s = 0$ is located at $x = 0$. In Fig. 3 this solution is shown as $LNN'R$, with all curves lying in the plane $w = 0$. The solution in the physical plane x, t is shown in Fig. 4. Each rarefaction fan extends right up to the shock, which therefore has one characteristic parallel to it on each side; this is the dividing case between an undercompressive and an overcompressive shock.

If w is allowed to be nonzero, another solution can be obtained by following the rarefaction curves only as far as M, M', where $u_M = u_{M'} = 0$, $(x/t)_M = -2J_s$, $(x/t)_{M'} = -2J_f$, and then linking these states by an Alfvén wave at $x/t = 0$. In fact, an infinite family of solutions can be found, as indicated in Fig. 4.

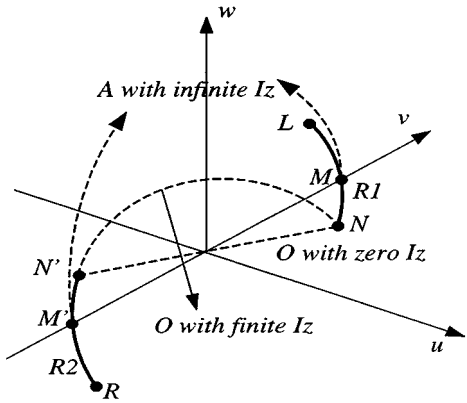

FIG. 3. Reference states on a slow rarefaction-wave curve and multiple solutions for a Riemann problem $\mathbf{u}_L = -\mathbf{u}_R = (-0.44, 2.4, 0)$. The points NN' can be joined by profiles lying either in or out of the plane. The points MM' are joined by a semicircle that represents Alfvén wave (A).

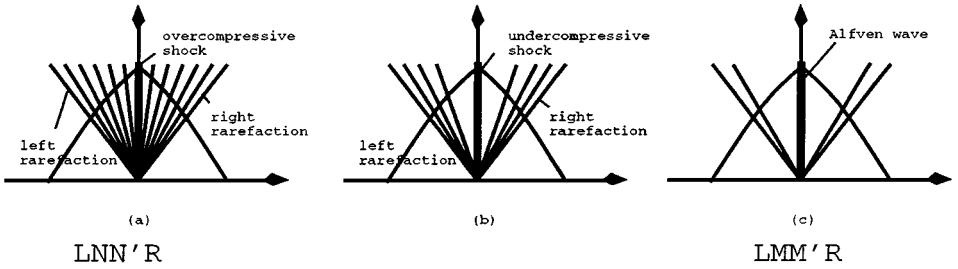

FIG. 4. (a)–(c). The multiple solutions in the physical plane (x, t).

All of the shocks involved are entropy-satisfying and have viscous profiles for the particular form of dissipations, $\mu \mathbf{I}\mathbf{u}_{xx}$. The solution,

$$\begin{aligned} u &= -u_0 \tanh(2u_0 x/\mu), \\ v &= -v_0 \tanh(2u_0 x/\mu) + C w_0 \operatorname{sech}(2u_0 x/\mu), \\ w &= -w_0 \tanh(2u_0 x/\mu) - C v_0 \operatorname{sech}(2u_0 x/\mu), \end{aligned} \tag{23}$$

represents a transition between states $\mathbf{u}_R = -\mathbf{u}_R = (u_0, v_0, w_0)$, provided

$$C^2 = 1 + \frac{(c-2)u_0^2}{v_0^2 + w_0^2}.$$

These profiles exist both for overcompressive shocks $(r_0/u_0) < \sqrt{c}$ and for undercompressive shocks $(r_0/u_0) \geq \sqrt{c}$.

Without loss of generality, let $w_0 = 0$, so that the wave is polarized in the x, y plane. Then, a transverse field moment is

$$I_z = -C(\mu\pi/2)\frac{v_0}{u_0} \quad \text{or} \quad I_z^2 = \frac{\pi^2\mu^2}{4}\left(\frac{v_0^2}{u_0^2} + c - 2\right). \tag{24}$$

A shock of this form can be used to join any point on the segment MN to its reflection in the origin, so completing a Riemann solution. The path includes a semi-elliptical trajectory outside the plane $w = 0$ that is defined by the viscous profile (23). The associated value of I_z increases from $\pi\mu\sqrt{(c-1)/2}$ at NN' to infinity at MM', this latter limit being the Alfvén wave. Being linearly degenerate this wave has no true travelling waveform, but is asymptotically infinite in extent. (The width of the waves can be measured in terms of μ/μ_0.) Note that for the path NN' a second path with $I_z = 0$ exists, corresponding to the planar solution.

3. NUMERICAL SCHEMES BASED ON WELL-POSED RIEMANN PROBLEMS

3.1. *Godunov's Method*

First, we consider Godunov-type methods. The Godunov numerical flux can be defined as

$$\mathbf{F}(\mathbf{u}_l, \mathbf{u}_r) = \mathbf{f}(\mathbf{u}^*(\mathbf{u}_l, \mathbf{u}_r)), \tag{25}$$

where $\mathbf{u}^*(\mathbf{u}_l, \mathbf{u}_r)$ is the intermediate state $\mathbf{u}(0)$ arising in the similarity solution $\mathbf{u}(x/t)$ of the Riemann problem, defined as an initial discontinuity ($\mathbf{u}_l$ for $x \le 0$, $\mathbf{u}_r$ for $x > 0$). The Godunov method is clearly ambiguous if the Riemann problem is ill-posed.

Here, we propose a new way to determine the intermediate state $\mathbf{u}(0)$. The basic idea is first to solve the planar Riemann problem (which is well-posed), and then to insert an Alfvén wave to deal with the rotation. In this framework, the magnetic field moments can be dealt with more naturally. Furthermore, the indeterminacy of v', w' in (6) will disappear.

The new scheme can be summarized as follows. Let us consider two solutions to the model Riemann problem with data (u_l, v_l, w_l), (u_r, v_r, w_r) of the conservation laws (2). We begin by solving the planar Riemann problem with data (u_l, r_l), (u_r, r_r), where

$$r_l^2 = v_l^2 + w_l^2, \tag{26}$$

$$r_r^2 = v_r^2 + w_r^2. \tag{27}$$

We can either choose to solve the problem in which r_l, r_r have the same sign, or else the problem in which they have opposite sign. In the first case, it can be shown that the path joining the left and right states always contains a unique point for which $x/t = 2u$ and where an Alfvén wave can be inserted to realign the left and right field orientations with an arbitrary adjustment. The second case always contains an intermediate shock that reverses the sign of r. The sign of $x/t - 2u$ changes across this shock and nowhere else, so there is nowhere to insert an Alfvén wave, and no way to realign the field directions (unless by 180°). We therefore choose the first strategy, with $r_l r_r > 0$. If $r_l = r_r = 0$, the resulting equation will simply be a scalar conservation law for u.

There is one remaining ambiguity. The sense of the rotational discontinuity (clockwise or anti-clockwise) is unresolved, and even its magnitude contains an arbitrary multiple of 2π. However, for the ideal problem, the representation in physical space is unaffected. Therefore, this form of the Riemann solution defines a unique numerical flux.

3.2. *Roe's Scheme*

Solving the MHD Riemann problem exactly turns out to be impractical, since even under an evolutionary condition it involves too many cases (the waves on either side of the contact may be S_1S_2, S_1R_2, R_1R_2, R_1S_2, S_1, S_2, R_1, R_2, each of these with or without an Alfvén wave). Thus we will be forced to use some approximations in MHD and therefore develop them also for the model problem.

In Roe's approximate Riemann solver [35], $\hat{\mathbf{u}}(x, t)$ is determined by solving a constant coefficient linear system of conservation laws,

$$\hat{\mathbf{u}}_t + \hat{A}(\mathbf{u}_l, \mathbf{u}_r)\hat{\mathbf{u}}_x = 0. \tag{28}$$

If $\hat{A}$ has eigenvalues $\hat{\lambda}_i$ and right eigenvectors $\hat{\mathbf{r}}_i$, and if we decompose $[\mathbf{u}] = \sum \hat{a}_i \hat{\mathbf{r}}_i$, then we have ($\xi = x/t$)

$$\hat{\mathbf{u}}(\xi) = \mathbf{u}_l + \sum_{\hat{\lambda}_i < \xi} \hat{a}_i \hat{\mathbf{r}}_i = \mathbf{u}_r - \sum_{\hat{\lambda}_i > \xi} \hat{a}_i \hat{\mathbf{r}}_i. \tag{29}$$

If some conditions are satisfied on $\hat{A}$, the numerical flux becomes

$$\mathbf{F}_{j+1/2} = \mathbf{f}(\mathbf{U}_j) + \sum_{\lambda_i<0} (\hat{\lambda}_i \hat{a}_i \hat{\mathbf{r}}_i)_{j+1/2}, \tag{30}$$

$$= \mathbf{f}(\mathbf{U}_{j+1}) - \sum_{\lambda_i>0} (\hat{\lambda}_i \hat{a}_i \hat{\mathbf{r}}_i)_{j+1/2}, \tag{31}$$

$$= \frac{1}{2}(\mathbf{f}(\mathbf{U}_j) + (\mathbf{f}(\mathbf{U}_{j+1})) - \frac{1}{2}\sum_i (|\hat{\lambda}_i| \hat{a}_i \hat{\mathbf{r}}_i)_{j+1/2}, \tag{32}$$

$$= \frac{1}{2}(\mathbf{f}(\mathbf{U}_j) + (\mathbf{f}(\mathbf{U}_{j+1})) - \frac{1}{2}|A(\widehat{\mathbf{U}}_{j+1/2})|(\mathbf{U}_{j+1} - \mathbf{U}_j). \tag{33}$$

In these equations, the hat represents Roe's average. However, because the model problem has only quadratic nonlinearity these are here just arithmetic means:

$$\bar{u} = \frac{1}{2}(u_l + u_r), \quad \bar{v} = \frac{1}{2}(v_l + v_r), \quad \bar{w} = \frac{1}{2}(w_l + w_r). \tag{34}$$

However, to create an approximation to the solver discussed in the previous section, we do not implement the method here in precisely this way; in particular, we do not employ the above averages. We take, instead, coplanar data (u_l, r_l), (u_r, r_r) and solve the approximate coplanar problem with

$$\bar{u} = \frac{1}{2}(u_l + u_r), \quad \bar{r} = \frac{1}{2}(r_l + r_r), \tag{35}$$

When the left and right states are separated by close to 180° this form of averaging is very different from the previous one.

Finally, the direction of the stationary state, ϕ^* is taken to be ϕ_l if the Alfvén wave has positive speed, and ϕ_r if the Alfvén wave has negative speed, i.e.,

$$\phi^* = \frac{1}{2}(1 + \mathrm{sign}(\lambda_a^*))\phi_l + \frac{1}{2}(1 - \mathrm{sign}(\lambda_a^*))\phi_r. \tag{36}$$

ϕ^* is undetermined if $u^* = 0$; but in that case the fluxes in (3) do not depend on ϕ^*. Specifically, if the Riemann flux for the coplanar problem is

$$\mathbf{f}_C^* = \begin{pmatrix} f_1^* \\ f_2^* \end{pmatrix} \tag{37}$$

then the Riemann flux for the noncoplanar problem is

$$\mathbf{f}_N^* = \begin{pmatrix} f_1^* \\ f_2^* \cos\phi^* \\ f_2^* \sin\phi^* \end{pmatrix}. \tag{38}$$

Alternatively, one may work with (u, r, ϕ) as the unknowns.

3.3. *Higher-Order Accuracy*

Most of procedures developed for higher accuracy can be applied to this method. For example, the MUSCL approach [40] and flux-limited methods can be used to obtain second-order accuracy. In this study, the following second-order space- and time-accurate upwind scheme, Hancock's scheme, is used [25, 36]. After a step involving a propagation over a time step $\Delta t/2$,

$$\bar{\mathbf{U}}_j = \mathbf{U}_j^n - \frac{\Delta t}{2\Delta x}\left(\mathbf{F}_{j+1/2}^n - \mathbf{F}_{j-1/2}^n\right), \tag{39}$$

where $\mathbf{F}$ can be given from Eqs. (33), (36), and (38), second-order extrapolations are introduced to $\bar{\mathbf{U}}$,

$$\mathbf{U}_{j+1/2}^l = \bar{\mathbf{U}}_j + \frac{1}{2}\mathbf{B}^l\left(\mathbf{U}_j^n - \mathbf{U}_{j-1}^n\right), \tag{40}$$

$$\mathbf{U}_{j-1/2}^r = \bar{\mathbf{U}}_j - \frac{1}{2}\mathbf{B}^r\left(\mathbf{U}_{j+1}^n - \mathbf{U}_j^n\right), \tag{41}$$

where

$$\mathbf{B}^{l,r} = \frac{1}{2}\left((1-\kappa)B(b^{l,r}) + (1+\kappa)b^{l,r}B\left(\frac{1}{b^{l,r}}\right)\right), \quad b^l = \frac{1}{b^r} = \frac{\mathbf{U}_{j+1}^n - \mathbf{U}_j^n}{\mathbf{U}_j^n - \mathbf{U}_{j-1}^n},$$

and the ratios in the last equation are defined componentwise. An extrapolation parameter κ and a symmetric limiter $B(b)$ are introduced. Then the final scheme is

$$\mathbf{U}_j^{n+1} = \mathbf{U}_j^n - \frac{\Delta t}{\Delta x}(\bar{\mathbf{F}}_{j+1/2} - \bar{\mathbf{F}}_{j-1/2}), \tag{42}$$

where $\bar{\mathbf{F}}_{j+1/2} = \mathbf{F}(\mathbf{U}_{j+1/2}^l, \mathbf{U}_{j+1/2}^r)$.

3.4. *Entropy Condition*

It is often necessary to modify Roe's approximate Riemann solver in order to remove entropy-violating shock waves. There exist various ways to do this [3, 24, 37], but it has not been found necessary to implement any of them in the present work. The MUSCL reconstruction tends to avoid most of the problems and leaves only very small "glitches" (see numerical experiment 1).

3.5. *Other Schemes*

From Eq. (38) the idea can be applied to other Godunov-type numerical schemes, for example, Marquina's scheme whose the flux function combines Roe's flux and a local Lax–Friedrichs flux [16]. Indeed, since it is based on a reformulation of the ideal equations, it can also be applied to other schemes such as the Lax–Wendroff scheme.

3.6. *Discussion*

For Riemann problems in which the left and right states have transverse vectors with significantly different orientations, the new schemes, either arising from Godunov's method or from Roe's, will give quite different fluxes from the old ones. The dissipation matrix $|A|$ in (33) can be determined to be, in the planar case, when $\lambda_s \le 0 \le \lambda_f$ (that is, when

$\overline{v}^2 \geq c\overline{u}^2$ and the flux is not wholly upwind),

$$|A| = \frac{1}{\left((c-1)^2\overline{u}^2 + 4\overline{v}^2\right)^{1/2}} \begin{pmatrix} 4\overline{v}^2 + 2c(c-1)\overline{u}^2 & 2(c+1)\overline{uv} \\ 2(c+1)\overline{uv} & 4\overline{v}^2 - 2(c-1)\overline{u}^2 \end{pmatrix}. \quad (43)$$

The trace of this matrix,

$$\mathrm{Tr}(|A|) = 2\left((c-1)^2\overline{u}^2 + 4\overline{v}^2\right)^{1/2},$$

is a measure of the numerical dissipation.

Consider left and right states comprising a rotational discontinuity $\mathbf{u}_L = (u_0, v_0)$, $\mathbf{u}_R = (u_0, -v_0)$. This is not, in general, an allowable discontinuity for either the planar or nonplanar problem. For the regular Roe solver, we have $\overline{u} = u_0$, $\overline{v} = 0$; hence, $\mathrm{Tr}(|A|) = 2|(c-1)u_0|$. Whereas for the modified solver we have $\overline{u} = u_0$, $\overline{v} = v_0$; hence, $\mathrm{Tr}(|A|) = 2((c-1)^2u_0^2 + 4v_0^2)^{1/2}$ which is greater than the regular dissipation by a factor of at least $(c+1)/(c-1)$. Therefore, we expect one feature of the new solver to be that it breaks up nonphysical discontinuities more rapidly.

Another aspect of the modified solver can be seen by considering data such that $\mathbf{u}_L = -\mathbf{u}_R$. For the old solver, the mean state is $\overline{u} = \overline{v} = 0$, and $|A|$ vanishes, whereas with the new solver, $|A|$ becomes a diagonal matrix $\mathrm{diag}(2|v_0|, 2|v_0|)$.

We now conduct some numerical experiments to observe the effects of these differences.

4. NUMERICAL RESULTS

The evolution of initial discontinuities predicted in Section 3 will be investigated by an upwind scheme using either a conventional Roe's solver (34) or the modified scheme (35). In all cases, $c = 3$, a grid of 200 points with $\Delta x = 0.005$ and the CFL number 0.5 are used. For second-order schemes, one-sided extrapolation $\kappa = -1$ and minmod limiter $B(b) = \max(0, \min(1, b))$ are used. The analytical solutions are described in Section 2.4 and are denoted by solid lines in Figs. 5–8.

4.1. *Behavior at a Sonic Point*

The first test problem intends to check the performance of the MUSCL scheme for data featuring an entropy-violating shock. The initial discontinuity is a fast switch-off expansive shock defined as $\mathbf{u}_L = (-u_0, 0, 0)$, $\mathbf{u}_R = (u_0, 2u_0, 0)$, $u_0 > 0$. The corresponding physical solution consists of slow and fast rarefaction waves. The slow rarefaction wave turns into fast one at $((1 - 5^{1/2})/2)u_0$. Numerical results in the physical space $u(x)$ and in the state space $v(u)$ are shown in Figs. 5a and b. Without any fix, the first-order scheme leads to a fast expansive shock. On the other hand, the MUSCL-type second-order scheme produces a numerical solution very close to the analytical solution, without the help of any sonic fix.

4.2. *A Problem with No Unique Solution*

The next problem is chosen for the purpose of investigating which solutions among the multiple ones discussed in Section 2.4 will be obtained by the new scheme. The initial discontinuity is an entropy-violating shock defined as $\mathbf{u}_L = -\mathbf{u}_R = (-0.44, 2.4, 0)$. The analytical solution is C_1C_2 when $I_z = 0$ ($LNN'R$ in Figs. 3 and 4) and R_1AR_2 when I_z

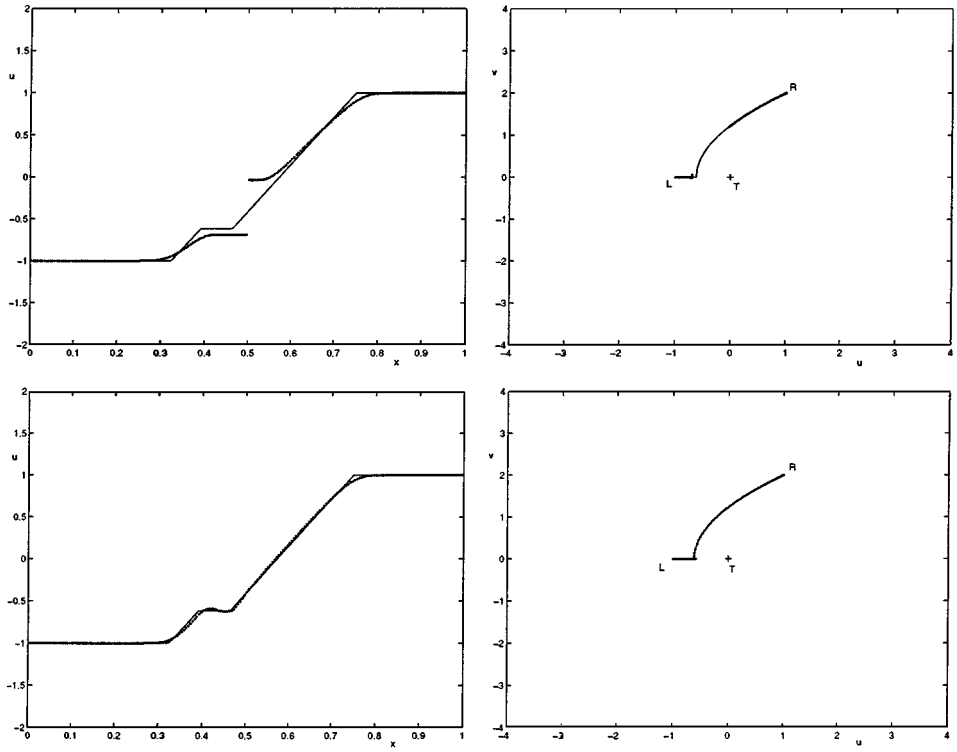

FIG. 5. Results for a test problem $\mathbf{u}_L = (-u_0, 0, 0)$, $\mathbf{u}_R = (u_0, 2u_0, 0)$, $u_0(=1) > 0$ by the new upwind scheme with Roe's solver: (a) first-order scheme without a sonic fix (top); (b) MUSCL-type second-order scheme without a sonic fix (bottom).

becomes infinity ($LMM'R$ in Figs. 3 and 4). We stress, however, that these calculations do not resolve the internal structures or compute the dissipative terms, so that I_z for these ideal calculations remains zero. Figure 6 shows that the conventional scheme actually yields neither of the above solutions but, instead, yields an R_1XR_2 configuration involving II $\rightarrow$ III intermediate shock with a larger entropy-production rate. On the other hand, the new scheme yields R_1AR_2 configuration involving Alfvén wave with a smaller entropy-production rate, which is shown in Fig. 7. The perfect resolution of this wave is due to its being stationary with respect to the grid. Other properties are similar to the result by the conventional scheme.

This test provides an example where the numerical solution is shown to be subject to the method used for defining interface fluxes, in this case by defining the average state. Therefore, we may build schemes in which different sets of Riemann solution are allowed. Here, it turns out that one tends to produce the intermediate-time solution, while another tends to generate the large-time solution.

4.3. *Rotational Discontinuity*

At this stage, it may be instructive to check the evolution of the rotational discontinuity. The initial discontinuity is given as $\mathbf{u}_L = (0.19, 1.8, 0)$, $\mathbf{u}_R = (0.19, -1.8, 0)$. The analytical solution [31] to the planar problem is a fast rarefaction followed by a slow compound wave, C_1R_2. Four equations (10)–(12) and (16) will determine two intermediate states uniquely. The three waves, a slow rarefaction, a slow intermediate shock, and a fast

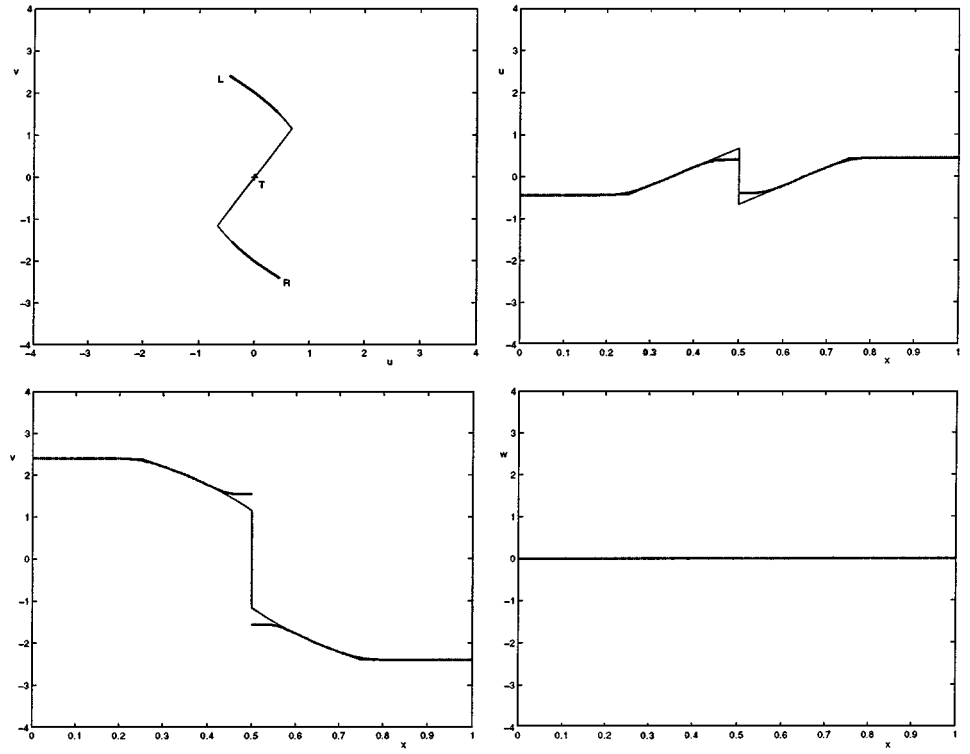

FIG. 6. Results for a Riemann problem $\mathbf{u}_L = -\mathbf{u}_R = (-0.44, 2.4, 0)$ by the regular version of Roe's solver in a second-order upwind method.

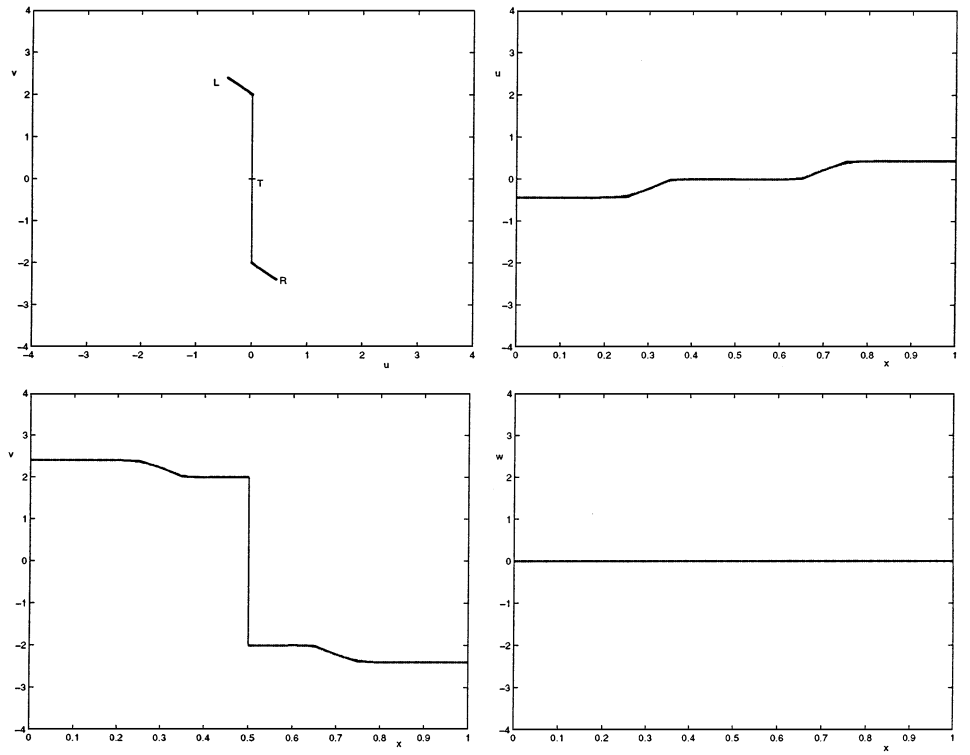

FIG. 7. Results for a Riemann problem $\mathbf{u}_L = -\mathbf{u}_R = (-0.44, 2.4, 0)$ by the new version of Roe's solver in a second-order upwind method.

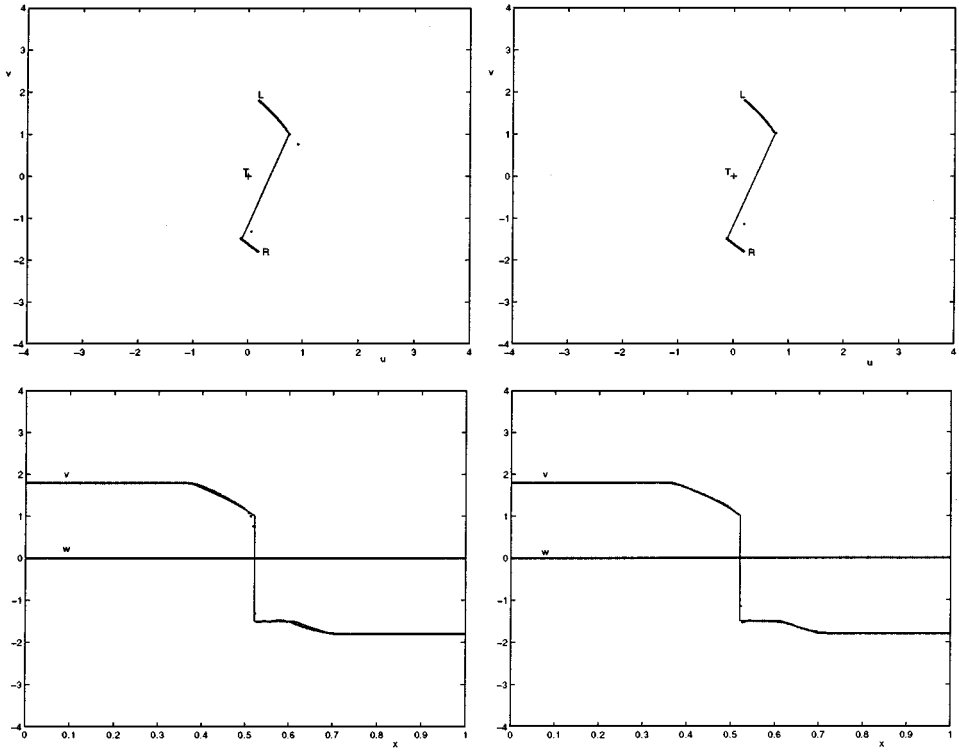

FIG. 8. Results for a Riemann problem of rotational discontinuity $\mathbf{u}_L = (0.19, 1.8, 0)$, $\mathbf{u}_R = (0.19, -1.8, 0)$: (a) conventional second-order upwind scheme (left half); (b) new second-order upwind scheme (right half).

rarefaction, are defined by four regions, $(x/t)_L = -2.86$, $(x/t)_{M,M'} \simeq 0.4608$ and 2.542, and $(x/t)_R = 4.38$.

Figures 8a and b show the results by the conventional and the new second-order upwind schemes. The results show excellent shock-capturing capability without spurious oscillations. Both schemes destroy the rotational discontinuity and converge to the analytical solution, but the new scheme yields a slightly better result. Here, it should be mentioned that even though the new scheme is built using only conventional evolutionary waves, the solution produces a nonevolutionary intermediate shock embedded in the compound wave. That is to say, it allows nonevolutionary waves to persist if, as here, they are constrained by symmetry to do so. And when they are present, they are well-resolved.

4.4. *Slightly Nonplanar Data*

Up to now, we considered only coplanar Riemann problems. Even though these have served to explore the MHD singularities, they are probably rare in practice. Thus the problems of more interest will be ones for which the differences in orientation are close to multiples of π. In Fig. 9, such a problem is studied by applying a small rotational disturbance to upstream and downstream states. Initially, the discontinuity is defined as $\mathbf{u}_L = -\mathbf{u}_R = (0.9375, 0.5, 0.0)$. This is preserved as a stable numerical solution by the regular scheme, although the modified scheme breaks it up immediately into an S_1AS_2 configuration, as seen in the right-hand figures. Then just after 300 iterations ($t = t_0$, labelled

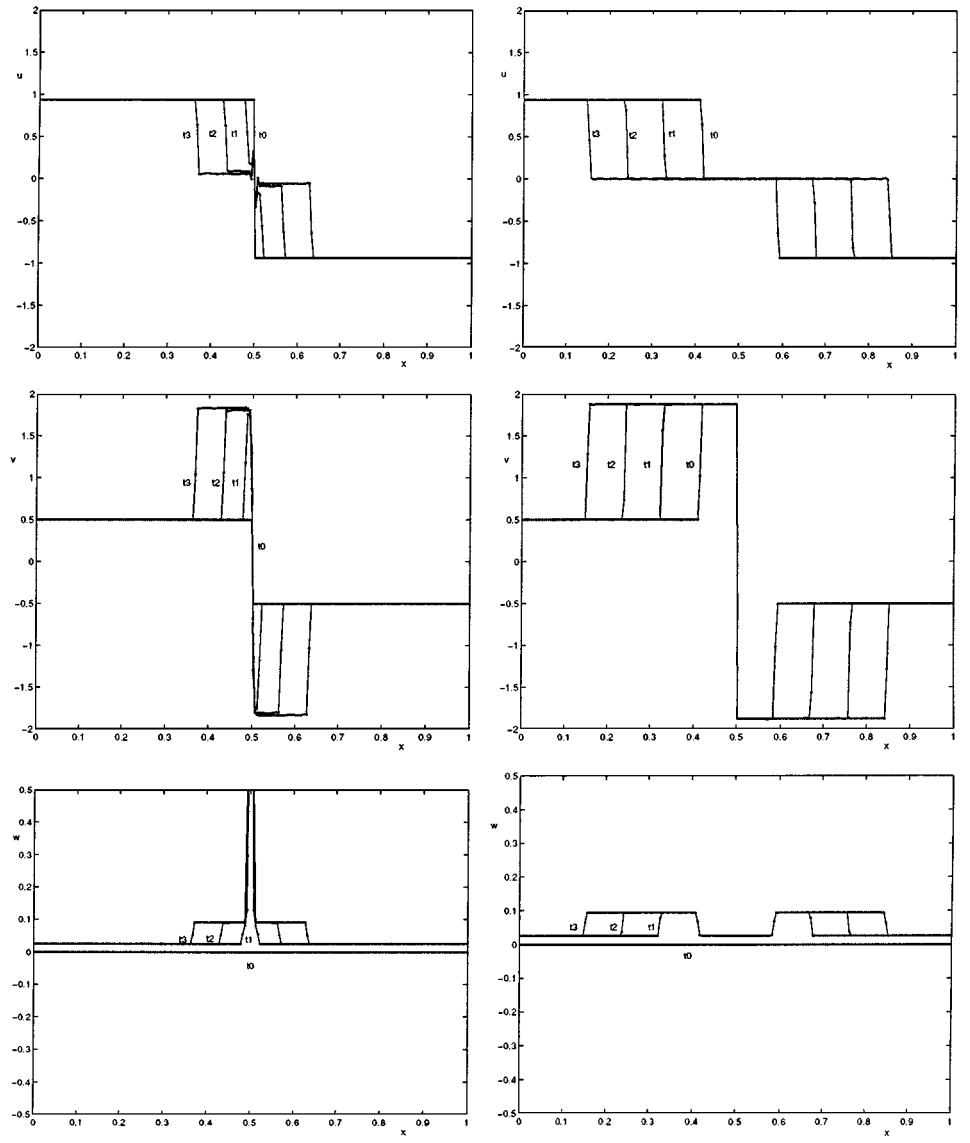

FIG. 9. Results for a noncoplanar Riemann problem $\mathbf{u}_L = -\mathbf{u}_R = (0.9375, 0.5, 0.0)$. t_0, t_1, t_2, t_3 indicate the time after 300, 600, 900, 1200 iterations. Rotational disturbance $w = 0.025$ is applied at t_0: (a) conventional second-order upwind scheme (left half); (b) new second-order upwind scheme (right half).

as t_0 in Fig. 9), a rotational disturbance $w = 0.025$ is added everywhere, so that the flow is no longer coplanar. The results are shown in the physical spaces $u(x)$, $v(x)$, and $w(x)$.

With the new scheme the S_1AS_2 configuration persists and the perturbation is incorporated smoothly. With the regular scheme the transition is slower and far less clean, featuring a time-dependent intermediate shock that eventually converges to an Alfvén wave. One of the differences with the new scheme is the existence of a spike in w. It does not disappear even in very large times and actually its amplitude increases.

In this case, the values of v either side of the Alfvén wave can be calculated by the Hugoniot relation as $v \simeq \pm 1.877$, something that the new scheme predicts more accurately

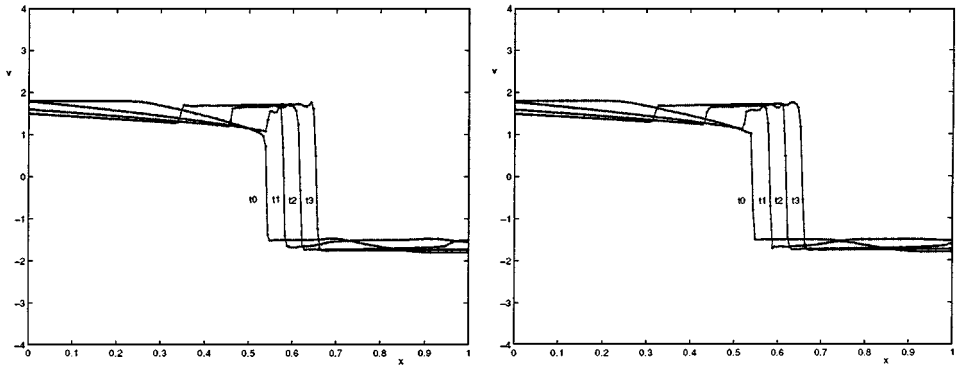

FIG. 10. Results for a noncoplanar Riemann problem $\mathbf{u}_L = (0.19, 1.8, 0.0)$, $\mathbf{u}_R = (0.19, -1.8, 0.0)$. t_0, t_1, t_2, t_3 indicate the time after 200, 400, 600, 800 iterations. Rotational disturbance $w = 0.09$ is applied at t_0: (a) conventional second-order upwind scheme (left); (b) new second-order upwind scheme (right).

than the old one. From this experiment, it is clear that the new scheme is more efficient than the conventional one in converging to the large-time solution.

4.5. *Perturbation of a Rotational Discontinuity*

In Fig. 10, another similar case is studied that involves the perturbation of 180° rotational discontinuity. The initial discontinuity is given as $\mathbf{u}_L = (0.19, 1.8, 0.0)$, $\mathbf{u}_R = (0.19, -1.8, 0.0)$. The exact solution for this planar problem is a slow compound wave formed from a slow rarefaction and an intermediate shock. This solution is seen labelled as t_0 in Fig. 10. At time t_0, the rotational disturbance $w = 0.09$ is added. Similarly to the previous results, the slow intermediate shock embedded in the compound wave is broken up into an Alfvén wave and left-running waves. This time there is little difference between the two sets of results. Notice that those left-running waves decay very slowly.

4.6. *A Viscous Calculation*

The last problem is considered in order to justify the new theory on the evolution of MHD shock waves. We consider a I → IV (overcompressive) intermediate shock ($\mathbf{u}_L = -\mathbf{u}_R = (0.9375, 0.5, 0)$, the same case that was treated ideally in Section 4.4) for which an exact viscous profile can be obtained from (23). We discretized the nonideal equation

$$\mathbf{u}_t + \mathbf{f}_x = \mu \mathbf{I} \mathbf{u}_{xx}$$

using the Lax–Wendroff method with extremely fine grids. We used $\mu = 0.002$ and 1000 grid points. This solution proved to be numerically stable.

Then we reran the computation with the same perturbation as in the ideal case $w = 0.025$, and the outcome is shown in Fig. 11. Here the initial data is labelled as t_0. After 1000 timesteps (label t_1) the internal structure of the initial profile has changed considerably (see in particular the phase-space (u, v) and (v, w) plots). However, the appearance in physical space $u(x)$ shows little change. After 5000 iterations (label t_2) the internal profile is approaching its asymptotic limit (a semicircle in (v, w)) and simultaneously the shocks start to form and move outward. After 15000 timesteps (label t_3) the picture is almost fully developed but decay of the central discontinuity is still not complete. The

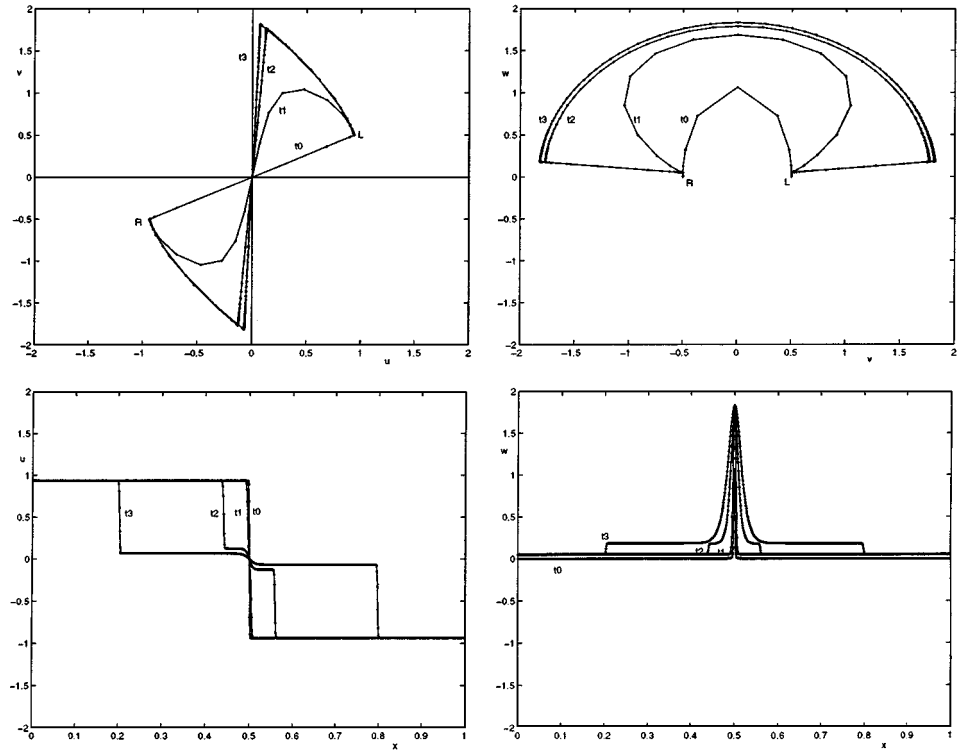

FIG. 11. Numerical experiments for nonideal problem $\mathbf{u}_L = -\mathbf{u}_R = (0.9375, 0.5, 0)$, $\mu = \eta = 0.002$ by the Lax–Wendroff method with a very fine grids (1000 grid points). t_0, t_1, t_2, t_3 indicate the time after 0, 1000, 5000, 15000 iterations. Initial viscous profiles at time t_0 and the evolution under noncoplanar variation are presented. Rotational disturbance $w = 0.025$ is applied at t_0.

Alfvén wave continues to expand slowly in phase space toward the profile predicted by (23) ($u \equiv 0$, $v^2 + w^2 = \text{const}$).

The integral I_z, taken over any finite domain, grows through three effects that can be seen in the $w(x)$ plot: first, w grows in magnitude; second, the region occupied by the Alfvén wave broadens; and third, the shocks move out. The combined effect of all these must be that I_z grows linearly in time (20) but the first two effects dominate the early history, whereas the last effect dominates the late-time behavior. Looking back to Section 4.4 and Fig. 9, we see that the new scheme, without resolving any internal structures, enforced very effectively the late-time behavior. The ideal calculation, of course, does not reveal the time-dependent broadening of the Alfvén wave that must occur with any finite μ.

5. SUMMARY AND DISCUSSION

As a step towards further refining Godunov-type numerical schemes for the MHD equations, a model system that exactly preserves the hyperbolic singularities has been studied. With the help of recent analytical results on nonstrictly hyperbolic conservation laws, a class of well-posed Riemann problem is identified. Based on this a new way to define numerical fluxes on cell interfaces is proposed. Numerical experiments show that the new scheme is more efficient in calculating the large-time solution. But the scheme also captures

intermediate shocks where these are allowed by the analysis, for example, shocks causing a 180° rotation. Analysis confirms that these intermediate shocks have viscous profiles, implying that numerical realizations of nonevolutionary shocks are not a mere consequence of numerical artifacts or forbidden disintegration of waves.

Extension to the full MHD equations presents some technical challenges, of which the most obvious is that the full problem features, in general, two Alfvén waves, and hence, two possible places for rotation to take place. We hope to report on a solution to this problem in due course. It also remains to be seen whether the essentially one-dimensional analysis involved in Godunov-type methods will continue to pay dividends in two- and three-dimensional calculations.

Nevertheless, we expect that the issues raised by the present work will remain important. The MHD equations, unlike the Euler equations, have weak solutions that cannot be determined in ignorance of the dissipations involved. The form of numerical dissipation employed therefore can and does affect the selection of solutions. As always, one would like to employ the weakest dissipation that bestows stability. The dissipation in Godunov-type schemes is a matrix having rather subtle properties. The dissipation proposed here is actually stronger than that of the regular scheme when faced with inadmissible shocks. Our claim is that this can substantially accelerate the convergence of a code to those weak solutions that typify late times.

ACKNOWLEDGMENTS

This work was supported in part by National Science Foundation under Research Grant ATM-9318181. The first author acknowledges the support from National Research Council-(NASA GSFC) Research Associateship Program.

REFERENCES

1. A. I. Akhiezer, G. J. Lubarski, and R. V. Polovin, The stability of shock waves in magnetohydrodynamics, *Soviet Phys.-JETP* **8**, 507 (1959).
2. A. I. Akhiezer and R. V. Polovin, The motion of a conducting piston in a magnetohydrodynamic medium, *Soviet Phys.-JETP* **11**, 383 (1960).
3. N. Aslan and T. Kammash, Developing numerical fluxes with new sonic fix for MHD equations, *J. Comput. Phys.* **133**, 43 (1997).
4. J. Augustinus, K. A. Hoffmann, and S. Harada, Numerical solutions of ideal MHD equations for a symmetric blunt body at hypersonic speeds, AIAA-98-0850.
5. A. A. Barmin, A. G. Kulikovskiy, and N. V. Pogorelov, Shock-capturing approach and nonevolutionary solutions in magnetohydrodynamics, *J. Comput. Phys.* **126**, 77 (1996).
6. J. Bazer and W. B. Ericson, Hydromagnetic shocks, *Astrophys. J.* **129**, 758 (1958).
7. M. Brio and P. Rosenau, Evolution and stability of the MHD fast-intermediate shock wave, preprint, 1994.
8. M. Brio and C. C. Wu, An upwind differencing scheme for the equations of ideal magnetohydrodynamics, *J. Comput. Phys.* **75**, 400 (1988).
9. P. Cargo and G. Gallice, A Roe solver for the magnetohydrodynamics equations, *C.R. Acad. Sci. I-Math.* **320**, 1269 (1995).
10. P. Cargo and G. Gallice, Roe matrices for ideal MHD and systematic construction of Roe matrices for systems of conservation laws, *J. Comput. Phys.* **136**, 446 (1997).
11. J. K. Chao, L. H. Lyu, B. H. Wu, A. J. Lazarus, T. S. Chang, and R. P. Lepping, Observations of an intermediate shock in interplanetary space, *J. Geophys. Res.* **98**, 17443 (1993).

12. C. C. Conley and J. A. Smoller, On the structure of magnetohydrodynamic shock waves, *Comm. Pure Appl. Math.* **27**, 367 (1974).
13. W. Dai and P. R. Woodward, An approximate Riemann solver for ideal magnetohydrodynamics, *J. Comput. Phys.* **111**, 354 (1994).
14. W. Dai and P. R. Woodward, A simple Riemann solver and high-order Godunov scheme for hyperbolic systems of conservation laws, *J. Comput. Phys.* **121**, 51 (1995).
15. D. L. De Zeeuw, A. F. Nagy, T. I. Gombosi, K. G. Powell, and J. G. Luhmann, A new axisymmetric MHD model of the interaction of the solar wind with Venus, *J. Geophys. Res.* **101**, 4547 (1996).
16. R. Donat and A. Marquina, Capturing shock reflections: An improved flux function, *J. Comput. Phys.* **125**, 42 (1996).
17. H. Freistühler, Some remarks on the structure of intermediate magnetohydrodynamic shocks, *J. Geophys. Res.* **96**, 3825 (1991).
18. H. Freistühler and E. B. Pitman, A numerical study of a rotationally degenerate hyperbolic system. Part I. The Riemann problem, *J. Comput. Phys.* **100**, 306 (1992).
19. H. Freistühler and E. B. Pitman, A numerical study of a rotationally degenerate hyperbolic system. Part II. The Cauchy problem, *SIAM J. Numer. Anal.* **32**(3), 741 (1995).
20. H. Freistühler and P. Szmolyan, Existence and bifurcation of viscous profiles for all intermediate magnetohydrodynamic shock waves, *SIAM J. Math. Anal.* **26**(1), 112 (1995).
21. P. Germain, Shock waves and shock-wave structure in magneto-fluid dynamics, *Rev. Mod. Phys.* **32**(4), 951 (1960).
22. S. K. Godunov, Finite difference method for numerical computation of discontinuous solutions of the equations of fluid dynamics, *Mat. Sb.* **47**, 271 (1959).
23. T. Hada, Evolution of large-amplitude Alfvén waves in the solar-wind with beta-similar-to 1, *Geophys. Res. Lett.* **20**(22), 2415 (1993).
24. A. Harten and J. M. Hyman, Self-adjusting grid methods for one-dimensional hyperbolic conservation laws, *J. Comput. Phys.* **50**, 235 (1983).
25. C. Hirsch, *Numerical Computation of Internal and External Flows* (Wiley, New York, 1988).
26. E. Isaacson, D. Marchesin, B. Plohr, and B. Temple, The Riemann problem near a hyperbolic singularity: The classification of solutions of quadratic Riemann problems I, *SIAM J. Appl. Math.* **48**(5), 1009 (1988).
27. A. Jeffrey and A. Taniuti, *Non-linear Wave Propagation* (Academic Press, New York, 1964).
28. P. Lax, Hyperbolic system of conservation laws II, *Comm. Pure Appl. Math.* **10**, 537 (1957).
29. S. A. Markovskii and B. V. Somov, Magnetohydrodynamic discontinuities in space plasmas: Interrelation between stability and structure, *Space Sci. Rev.* **78**, 443 (1996).
30. R. S. Myong, Analytical results on MHD intermediate shocks, *Geophys. Res. Lett.* **24**(22), 2929 (1997).
31. R. S. Myong and P. L. Roe, Shock waves and rarefaction waves in magnetohydrodynamics. Part 1. A model system, *J. Plasma Phys.* **58**, 485 (1997).
32. R. S. Myong and P. L. Roe, Shock waves and rarefaction waves in magnetohydrodynamics. Part 2. The MHD system, *J. Plasma Phys.* **58**, 521 (1997).
33. L. P. O'Hare and J. D. Anderson Jr., Maneuvering a reentry body via magnetogasdynamic forces, AIAA-93-3202.
34. R. V. Polovin and V. P. Demutskii, Fundamentals of magnetohydrodynamics, Consultants Bureau, 1990.
35. P. L. Roe, Approximate Riemann solvers, parameter vectors, and difference schemes, *J. Comput. Phys.* **43**, 357 (981).
36. P. L. Roe, Characteristic-based schemes for the Euler equations, *Ann. Rev. Fluid Mech.* **18**, 337 (1986).
37. P. L. Roe, Sonic flux formulae, *SIAM J. Sci. Statist. Comput.* **13**, 611 (1992).
38. P. L. Roe and D. S. Balsara, Notes on the eigensystem of magnetohydrodynamics, *SIAM J. Appl. Math.* **56**(1), 57 (1996).
39. A. Tveito and R. Winther, The solution of nonstrictly hyperbolic conservation laws may be hard to compute, *SIAM J. Sci. Comput.* **16**(2), 320 (1995).
40. B. van Leer, Towards the ultimate conservative difference scheme, II. Monotonicity and conservation combined in a second-order scheme, *J. Comput. Phys.* **14**, 361 (1974).

41. M. H. P. M. van Putten, A numerical implementation of MHD in divergence form, *J. Comput. Phys.* **105**, 339 (1993).
42. B. L. Venable, D. A. Anderson, and D. R. Wilson, A numerical investigation of a shock-tube-driven conductivity channel, AIAA-96-4590-CP.
43. C. C. Wu, On MHD intermediate shocks, *Geophys. Res. Lett.* **14**(6), 668 (1987).
44. C. C. Wu, Intermediate shocks, *Phys. Scripta* **T60**, 97 (1995).
45. A. L. Zachary and P. Colella, A higher-order Godunov method for the equations of ideal magnetohydrodynamics, *J. Comput. Phys.* **99**, 341 (1992).